

RESEARCH PROJECT IN MECHATRONICS ENGINEERING

Final Research Report
The Perception of Biological Motion

Alan Chen

Project Report ME037-2022

Co-worker: Joseph Byrne

Supervisor: Dr. Luke Hallum

Department of Mechanical and Mechatronics Engineering
The University of Auckland

16 October 2022

THE PERCEPTION OF BIOLOGICAL MOTION

Alan Chen

ABSTRACT

The perception of biological motion (PoBM) is an evolutionary skill which has been developed as a survival trait. In more recent history, the underlying mechanisms which allow us to see this locomotion have become its own area of research within neuroscience and vision.

This project aimed to prove our hypothesis that the performance of the PoBM worsens as peripheral eccentricity increases. Human gait data was recorded in a motion capture lab before being processed and rendered in various configurations deemed necessary by the experimental design. These prepared experiments were then trialed on twelve students at the University of Auckland in a controlled, fair testing environment.

The resulting data provided several insights into the proposed hypothesis. Psychometric (WCDF) functions were fitted to the data for trials done in the fovea and periphery respectively. Bootstrapping was performed 1000 times to draw conclusions with appropriate statistical significance. Our trials produced mean values which suggest that recognition accuracy in the periphery is hindered markedly. On average, trials in the periphery require 7 more visible nodes on the PLW to gain equivalent recognition accuracy to the fovea.

The results also provided insight into interactions between viewpoint angle and peripheral eccentricity as it pertains to the performance of PoBM. Our trials suggest extremely high sensitivity for frontal viewpoints, regardless of peripheral eccentricity. In addition, we found that profile viewpoint recognition rates were far more accurate in the fovea. This provides a basis for potential future works to truly form solid conclusions.

DECLARATION

Student

I hereby declare that:

1. This report is the result of the final year project work carried out by my project partner (see cover page) and I under the guidance of our supervisor (see cover page) in the 2022 academic year at the Department of Mechanical and Mechatronics Engineering, Faculty of Engineering, University of Auckland.
2. This report is not the outcome of work done previously.
3. This report is not the outcome of work done in collaboration, except that with a potential project sponsor (if any) as stated in the text.
4. This report is not the same as any report, thesis, conference article or journal paper, or any other publication or unpublished work in any format.

In the case of a continuing project, please state clearly what has been developed during the project and what was available from previous year(s):

Signature:



Date: 10th October 2022

Supervisor

I confirm that the project work undertaken by this student in the 2022 academic year ~~is~~ / is not (strikethrough as appropriate) part of a continuing project, components of which have been completed previously. Comments, if any:

Signature:



Date: 10th October 2022

Table of Contents

Acknowledgements	1
Glossary of Terms	2
Abbreviations	2
1 Introduction	1
1.1 Overview	1
1.2 Objectives	1
2 Literature Review	2
2.1 Point Light Walker Origin	2
2.2 Viewpoint Dependency	2
2.3 Visual Degradation Tactics	4
2.4 Peripheral Vision	5
2.5 Gap Identification	6
3 Data Collection	7
3.1 Data Capture	7
3.2 Data Processing	8
3.3 PLW with Varying Viewpoint Angles	8
3.4 PLW with Visual Degradation	9
4 Experimental Methods	10
4.1 Experimental Matrix	10
4.2 Experimental Design	10
4.2.1 Test Environment	11
4.2.2 Test Procedure	12
5 Results and Discussion	13
5.1 Foveal vs. Peripheral Vision	13
5.1.1 Psychometric Functions	13
5.1.2 Bootstrapping	14
5.2 Viewpoint Angle vs. Peripheral Eccentricity	15
5.2.1 Psychometric Functions and Bootstrapping	15
6 Conclusion	17
7 Future Works	17
References	19
Appendix A The First Appendix	21
A.1 MATLAB Data Processing	21
A.2 Data Collection and Stimuli Construction	22
Appendix B Second Appendix	26
B.1 Viewpoint Graphs	26
B.1.1 Viewpoint Psychometric Functions	26
B.1.2 Viewpoint Bootstrapped Histograms	28

Appendix C MOCAP Lab	30
Appendix D Test Environment	31

List of Figures

Figure 1 Point light walker in a profile viewpoint angle	1
Figure 2 Typical motion trajectories of different joints provided by the kinetic-geometric models [1]	2
Figure 3 Visualisation for the experimental design in [2]	3
Figure 4 Joint trajectories: (a) Coherent point light walker (b) Scrambled point light walker [3]	4
Figure 5 Figure "morphing" between time intervals [4]	4
Figure 6 Density of colour-sensitive photoreceptors with respect to peripheral eccentricity	5
Figure 7 Results for three different subject (KW, HI, KY). Performance is plotted with respect to the size of the stimulus.	6
Figure 8 Velcro suit retro reflective node configuration (a) frontal node arrangement, (b) rear node arrangement	7
Figure 9 ViconNexus™ software GUI to visualise the PLW as it is being rendered	8
Figure 10 PLW with 28 visible nodes: (a) Angle = 0°, (b) Angle = 30°, (c) Angle = 60°, (d) Angle = 90°	9
Figure 11 PLW with 8 visible nodes: (a) Angle = 0°, (b) Angle = 30°, (c) Angle = 60°, (d) Angle = 90°	9
Figure 12 3D Experiment Matrix	11
Figure 13 (a) Chin brace set up to control the movement of the subject's head, (b) Fixation spot at 0 and 40 degrees to indicate peripheral eccentricities .	11
Figure 14 Flow diagram showing the designed test procedure. One full loop of this diagram indicates one completed trial in the overall block.	12
Figure 15 Visual diagram showing the progression of the trial loop.	12
Figure 16 Mean success rate as a function of number of nodes	13
Figure 17 Fitted psychometric functions to the 0 and 40 degree eccentricity data. Indicated by green markers are the critical thresholds of each curve (4.276 and 11.508).	14
Figure 18 Histograms showing the Gaussian distribution of critical thresholds across 1000 rounds of bootstrapping. A 0 degree eccentricity has a mean value of 4.275 nodes and a 40 degree eccentricity has a mean value of 11.519 nodes.	15
Figure 19 Raw data showing the success rate as a function of number of nodes for all four viewpoint angles	15
Figure B1 Psychometric functions between viewpoint angles of 0 and 30 degrees	26
Figure B2 Psychometric functions between viewpoint angles of 60 and 90 degrees	27
Figure B3 Bootstrapped histograms between viewpoint angles of 0 and 30 degrees	28
Figure B4 Bootstrapped histograms between viewpoint angles of 60 and 90 degrees	29
Figure C5 Motion capture lab at the University of Auckland	30
Figure C6 Vicon Nexus station which interfaces with the system which connects all the cameras within the lab	30
Figure D7 BCI Lab station where all trial experiments are done (note: lights switched off under normal test conditions)	31

List of Tables

Table 1	Independent Variables Table	10
Table 2	Mean critical threshold values for each combination of viewpoint angle and peripheral eccentricity.	16

Acknowledgements

I would like to take the time to show my appreciation for the following individuals:

- Dr. Luke Hallum, our supervisor: Thank you for the continuous support you have provided us over the course of this year. Your sage wisdom and advice guided us to where this project has ended up.
- Joseph Byrne, project partner: Thank you for your commitment to the project. It has been a pleasure to bounce ideas off you and work with someone as passionate as you. I think we are both proud of this project and where we have taken it.
- Jerry Zhang, Carl Tang, Kevin Lee, post-grad mentors: Thank you for your willingness to help in every situation. From helping us install Psychtoolbox in the BCI lab, to participating in our experimental trials, we appreciate the time you have given to us.
- Luke Patterson, Divya Roshinkumar, Joseph Darge, Bailey Sutton, Oscar Waston, etc., experimental trial participants: Thank you for taking the time to do our experiments. At times you focused for upwards of 30 minutes. Some of you also came back for revised versions of our experiments. Joe and I have very much appreciated how accommodating you have been with your time.
- Emanuele Romano, lab technician: Thank you for your help training us with the motion capture lab and organising the treadmill. All this work made the collection of our data so much easier.

Glossary of Terms

Azimuth	The horizontal angle in a spherical co-ordinate system
Biological Motion	Motion which occurs from actions performed by biological organisms. Animals have adapted to recognise these actions through understanding the underlying patterns and mechanisms
Bootstrapping	A statistical procedure that resamples a single dataset to create many simulated samples
Elevation	The vertical angle in a spherical co-ordinate system
Fovea	The location in the retina where visual acuity is highest
Frontal Viewpoint	A 0° viewpoint angle in the azimuth direction
Peripheral Eccentricity	The angle at which an object is located in the peripheral vision
Peripheral Vision	Vision that occurs outside of the point of fixation, i.e. vision of things outside of the centre of gaze
Profile Viewpoint	A 90° viewpoint angle in the azimuth direction
Psychometric Function	An inferential function which models the relationship between a physical stimulus and forced-choice responses in detection and discrimination tasks
Viewpoint Angle	The angle at which an observer sees an object

Abbreviations

4AFC	Four Alternative Forced Choice
MCC	Mathew's Correlation Coefficient
MOCAP	Motion Capture
PLW	Point Light Walker
PoBM	Perception of Biological Motion
WCDF	Weibull Cumulative Distribution Function

1. Introduction

1.1 Overview

Studies have shown that the human brain is able to characterise the motion of a biological organism based solely on the movement of the main joints in its physiology [1] (Figure 1). By placing simple point light markers on these locations, a convincing portrayal of a subject's locomotion can be provided. This phenomenon, which has become a neuroscientific field of study, is known as the perception of biological motion (PoBM). It is a skill which has been evolved by humans over thousands of years and is credited as a survival trait. Despite this, very little is known about how the underlying mechanisms actually work.

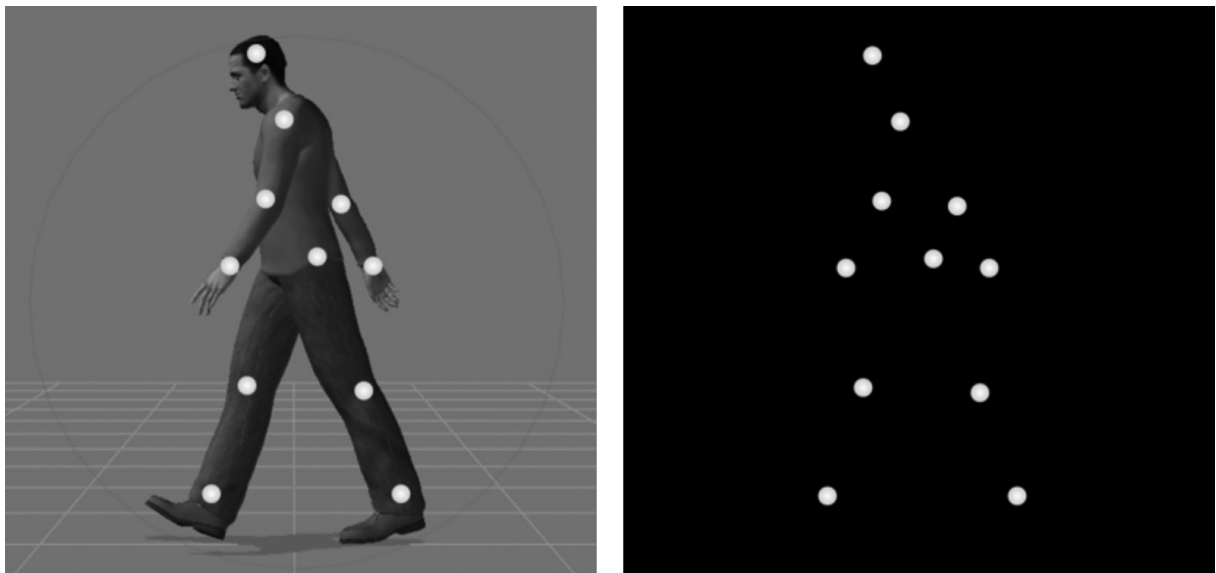


Figure 1 Point light walker in a profile viewpoint angle

Subsequent pieces of literature have investigated how features like gender [5–7], viewpoint angles [2, 8] and emotion [9] are conveyed. These alternative approaches to studying the perception of biological motion provided inspiration for the direction of our project. We aimed to investigate how changing degrees of peripheral eccentricity affects the performance of the PoBM in humans. To do this we applied engineering practices in order to quantify these influences in meaningful ways. From a neuroscience standpoint, we wish to contribute to the limited pool of literature regarding the PoBM and vision science as a whole.

1.2 Objectives

The main objectives of this project were to investigate and quantify:

- The effects *peripheral vision* have on the performance of the PoBM
- The effects different *viewpoint angles* have on the performance of the PoBM
- The interaction between *peripheral vision* and *different viewpoint angles* and the effect this has on the performance of the PoBM

We hypothesised that **increasing peripheral eccentricity decreases the recognition accuracy of the PoBM.**

2. Literature Review

The following literature review provides an overview on the brief history of the study on the PoBM. We touch on previous point light walker (PLW) studies that have investigated how different viewpoint angles and visual degradation tactics impacted the performance of the PoBM. In addition, we will present literature that discusses peripheral vision, especially as it pertains to its interaction with biological motion.

2.1 Point Light Walker Origin

[1] presented the first ever PLW in 1973. Johansson, reduced human motion to just its main joints and proved that a vivid representation could still be preserved. He did this by illuminating as few as 10-12 elements across the human body. Parameters such as walking direction, speed and activity could be identified. Additionally, this PLW model allowed for analysis on the trajectory of individual nodes. He proposed kinetic-geometric models to describe the pendulum motion of joints during periodic movements like walking (Figure 2). Johansson proposed that the interaction between these may allow for the emergence of a new field of study in neuroscience. This inspired numerous subsequent papers which investigated the more nuanced mechanisms behind the PoBM.

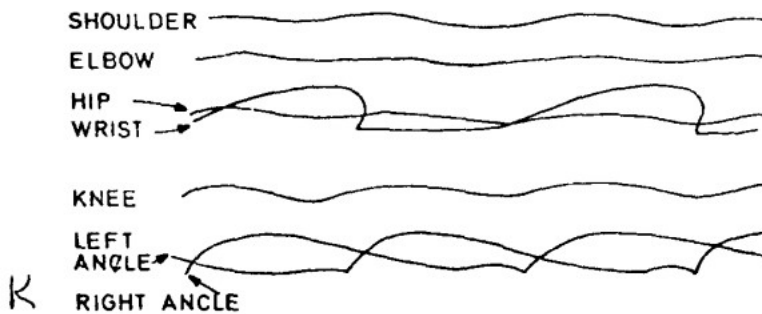


Figure 2 Typical motion trajectories of different joints provided by the kinetic-geometric models [1]

2.2 Viewpoint Dependency

The performance of the PoBM under varying viewpoint angles played a prevalent part in our experimental design. Several studies have been conducted to understand one's ability to identify biological motion [2, 3, 8] under these conditions. The research in this area places a focus on how perspectives (e.g. frontal, half-profile and profile view) effect one's recognition accuracy.

An investigation on self recognition versus recognition of others with the added variable of viewpoint angle was conducted in [2]. Two groups of twelve participants varying in age and gender were used as subjects in acquiring biological motion data. Of these 24, 20 were used later as observers. The population was comprised of eleven males and nine females ranging between 21 and 42 years old. All participants had been working at the Ruhr University of Bochum for 6 weeks, and thus were well acquainted. Data was collected via CCD cameras in a 3D motion capture laboratory. A point light configuration was used which consisted of 41 retro-reflective nodes, arranged methodically. Post processing removed translation motion and the data was fitted to a Fourier series [10] such that the locomotion could be looped continuously.

Their experimental design employed a 12-alternative forced-choice paradigm. Before the test, a list of 12 names of all the people to be presented were displayed to the trial subject.

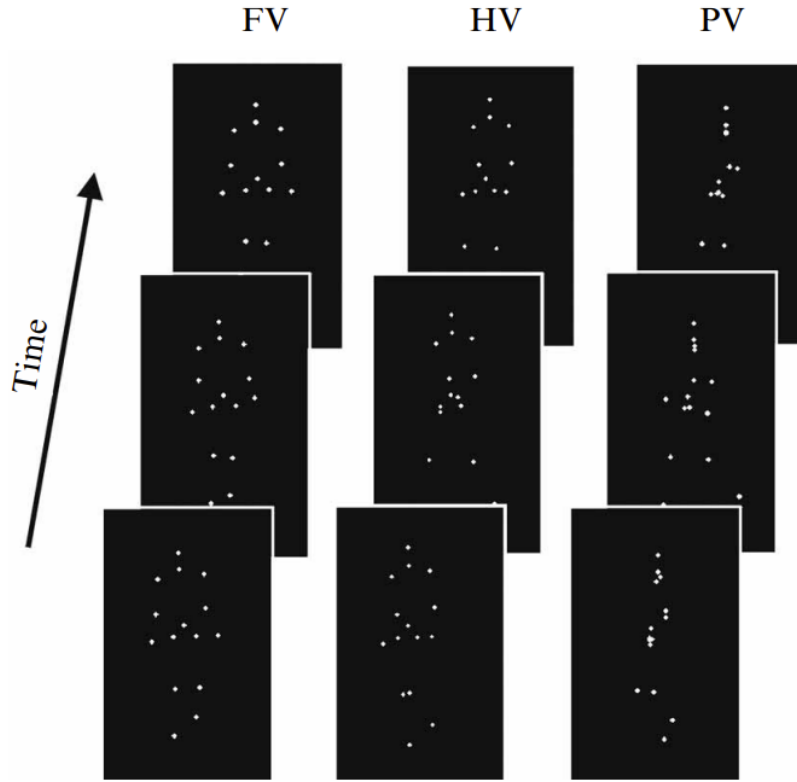


Figure 3 Visualisation for the experimental design in [2]

36 trials were split into 3 blocks, and their respective order were randomised between trials. A single block consisted of each of the 12 point light walker subjects gait representations, respectively. Each point light walker was shown in profile, half-profile and frontal view simultaneously (Figure 3). As a result, each subject observed 33 different gait patterns from other colleagues and 3 from his/her own. After being presented by the stimulus, the subject was prompted to answer which person they believe was shown.

After these experiments were conducted on the observers, data analysis was conducted. The resulting function provided a percentage score to quantify the subjects' ability to identify biological motion in each viewing angle. When viewing another individual's gait, the data provided mean successful recognition rates of 28.6%, 26.6% and 18.4% for frontal, half-profile and profile views respectively. When viewing ones own gait, the data provided mean successful recognition rates of 27.5%, 30% and 30% for front, half-profile and profile views respectively. They concluded that azimuth has no significant effect on the successful recognition of a subject.

Across all observations, they also concluded that the point light configuration provided insufficient information for recognition. Furthermore, we see that viewpoint angle only seemed to have a significant effect when observers are viewing another individuals biological motion. Specifically, frontal and half-profile views are identified more successfully and this is corroborated with data from one of Troje's later studies [11]. Here, they hypothesise that subjects have a heightened sense of awareness when someone is approaching them.

Additionally, [2] and [11] agree in that time exposure improves the ability to identify a specific gait. When provided with PLW subjects for a longer duration in time, subjects are able to score more accurately.

2.3 Visual Degradation Tactics

In an effort to quantify the effects of the different variables interacting with the perception of biological motion, the visibility of the point light walker data can be systematically manipulated. One can then obtain a psychometric function for an observer's sensitivity to the perception of biological motion.

One visual degradation tactic that has been implemented is previous studies is the addition of random extra dots [12]. This is a way of integrating noise such that the subject were "in a snowfall". They did this until they reached a threshold number of dots where observers could no longer accurately perceive biological motion. In this particular study done on an adult observer, the study found this threshold to be 86.86 dots.

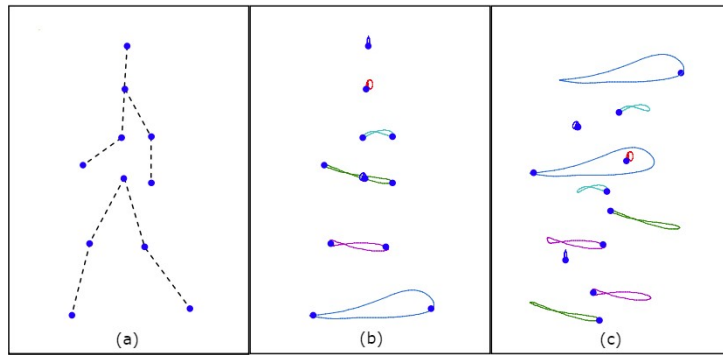


Figure 4 Joint trajectories: (a) Coherent point light walker (b) Scrambled point light walker [3]

Another approach to manipulating the point light walker is through superimposing it with scrambled walkers [3]. These scrambled walkers add random, but constant offsets to the location of single joint trajectories (Figure 11). This results in a walker with incoherent structure whilst preserving the local motion of joints. Troje et al. found that the general direction of motion could still be discerned despite the absence of a coherent figure. Additionally, they noted that the motion of the feet was most important for recognition over any other body part. They concluded that this effect is a product of the brain's heuristic ability to anticipate local trajectories based on its understanding of the kinetic-geometric models which describe the pendulum motion of joints.

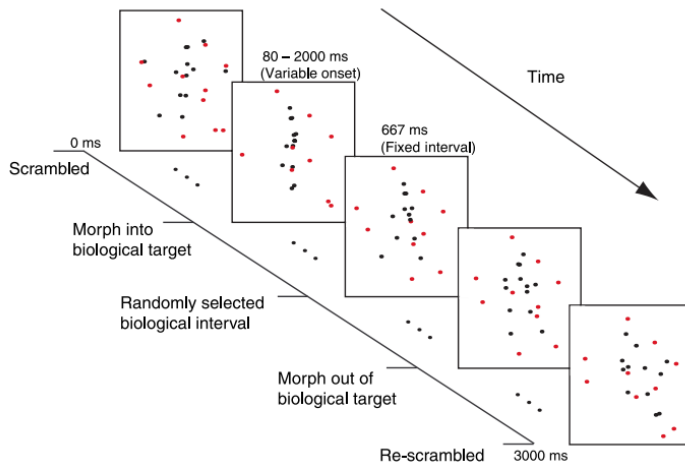


Figure 5 Figure "morphing" between time intervals [4]

A common method for manipulation is done by removing specific joints [13]. In previous studies this has been done as way of exploring their relative importance to the way we

comprise our perception of biological motion. This method has then been further iterated upon with a lifetime function. The effect can be described as a dynamic "jitter" of the position of the nodes on the limbs on a frame by frame basis. In [4], this procedure is implemented through 600 ms intervals.

2.4 Peripheral Vision

A large focus on our project is understanding the interaction peripheral vision has on our perception of biological motion. The prominence of this can be seen in common day to day scenarios that almost all humans go through [14, 15]. Activities such as walking through crowds are highly dependent on the perception of biological motion in the periphery.

When comparing peripheral vision to foveal vision more holistically, studies have found many differences. Scientifically these differences can be attributed to the fact that the fovea (region on the retina where light is focus) occupies 1% or less in surface area on the retina, but equates for 50% of visual cortex [16]. In addition to this, [17] found that the large proportion of colour-sensitive photoreceptors lie in the fovea (Figure 6). Anatomically, these are a few of the reasons for a lower overall acuity in the periphery.

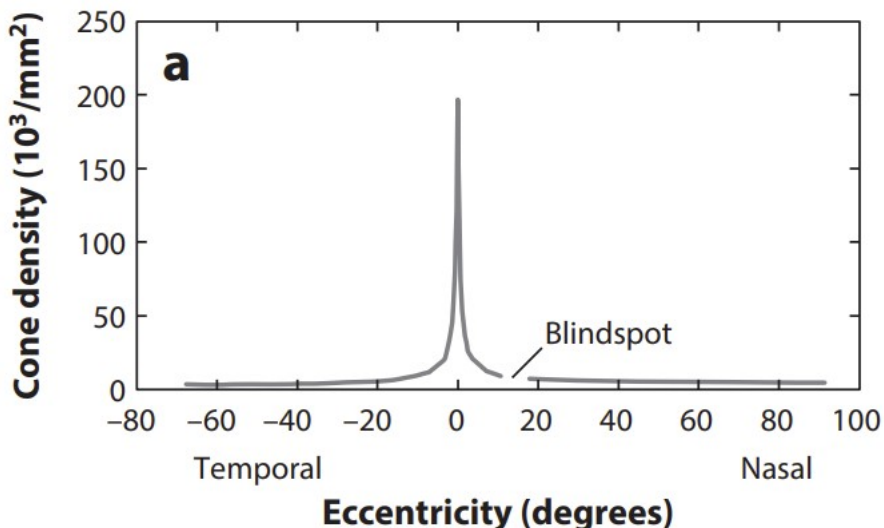


Figure 6 Density of colour-sensitive photoreceptors with respect to peripheral eccentricity

As it relates to the PoBM, very few studies have attempted to quantify the effects of peripheral eccentricity on the PoBM. [18] presents both the most related and relevant study for our review. In this study, a single viewpoint angle of five different activities (walking, running, jumping, kicking and throwing a ball) was presented to six subjects (two female, four male). In addition, an inverted version of each of these PLWs were presented. These animations were altered both in size and eccentricity. To achieve varying eccentricity levels, a fixation cross was shifted to the left of the screen while the stimuli remained at the centre of the screen. This allowed for the stimuli to form on the right side of the subject's field of vision.

Subjects were then seated a distance of 57 cm away from the monitor and their head movements were minimised using a head and chin rest. Trials were initiated by the press of a key. The subject would then be presented with two successive 800 ms samples of a PLW with a 500 ms interval period in between. One sample would display the normal biological motion sequence, while the other would present a scrambled one. Scrambled PLWs were generated by randomising the starting position of the visible nodes. Throughout the entire 800 ms, this configuration is held. The subjects were then asked to identify which of the two samples was unscrambled/scrambled.

The results of this 2 alternative forced choice task indicated that the performance of the PoBM varied with levels of eccentricity (Figure 7). It can be seen that a lower performance asymptote is obtained with increasing levels of eccentricity. This trend is consistent across all three subjects. The paper suggests that the most effective processing of biological motion is reserved for foveal vision.

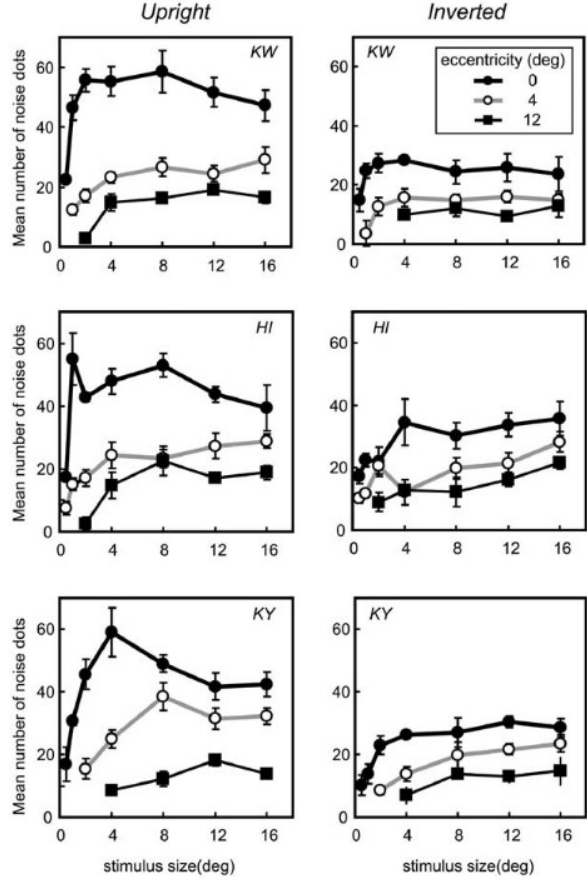


Figure 7 Results for three different subject (KW, HI, KY). Performance is plotted with respect to the size of the stimulus.

2.5 Gap Identification

A comprehensive literature review was conducted to provide insight into the protocols used for PoBM projects in previous studies. Through this process, we became aware of the novelty of our proposed project. As discussed, only one other study has truly attempted to investigate how peripheral vision affects the performance of the PoBM [18]. There exists several limitations within this piece of literature which warrants further research into this area. Firstly, only near peripheral eccentricities are tested (4° and 12°). Secondly, no testing was done on viewpoint dependency for the PoBM in peripheral vision. Therefore, we have gained significant evidence for the novel nature of the direction we took the project.

3. Data Collection

Data collection was conducted to obtain key joint trajectories during walking. These would then be used for rendering our own PLWs and manipulating it in unique ways defined by our experimental design. We captured the gait of a human volunteer subject and exported this data into MATLAB®. The tools we used within this software allowed us show PLWs in user defined viewpoint angles. Moreover, we were able to implement visual degradation tactics such as reducing the number of visible nodes and applying a node lifetime function.

3.1 Data Capture

The first step taken was collecting human gait data in the Mechanical department's state of the art motion capture (MOCAP) lab. The lab is equipped with 14 LiDAR cameras which interface with ViconNexus™ which is a data capture software designed for life sciences. We used the information these cameras received to develop a coherent 360° representation of the subject's motion.

For our captured data, we recorded a 22-year-old male's gait within the lab space. 28 carefully positioned retro-reflective nodes were placed on the velcro suit which he wore (Figure 8). These were used to represent the primary joints of the human physiology. To remove the translational element of the data, we had him walk on a treadmill. The treadmill was set to approximately 1.5 m/s - a typical walking speed at moderate pace.

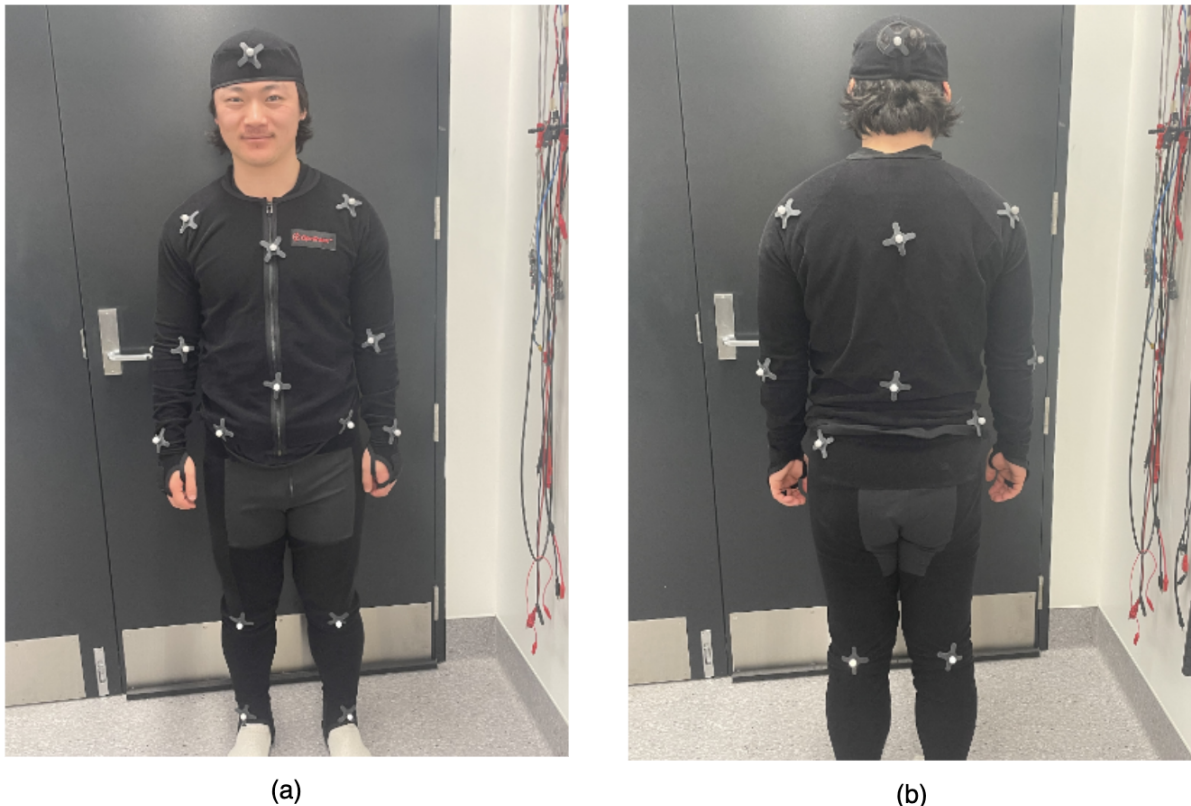


Figure 8 Velcro suit retro reflective node configuration (a) frontal node arrangement, (b) rear node arrangement

This subject was captured for a duration of 60 seconds. During this time, the LiDAR cameras were able to track the location of each individual retro reflective node. This 3D information is stored in ViconNexus™ which can be used for post-processing.

3.2 Data Processing

All trajectory data is initially stored within the ViconNexus™ software (Figure 9). For the purposes of our project, we selected to use MATLAB® for data manipulation. ViconNexus™ provides a class with many helpful methods to extract this data in various ways into the workspace.

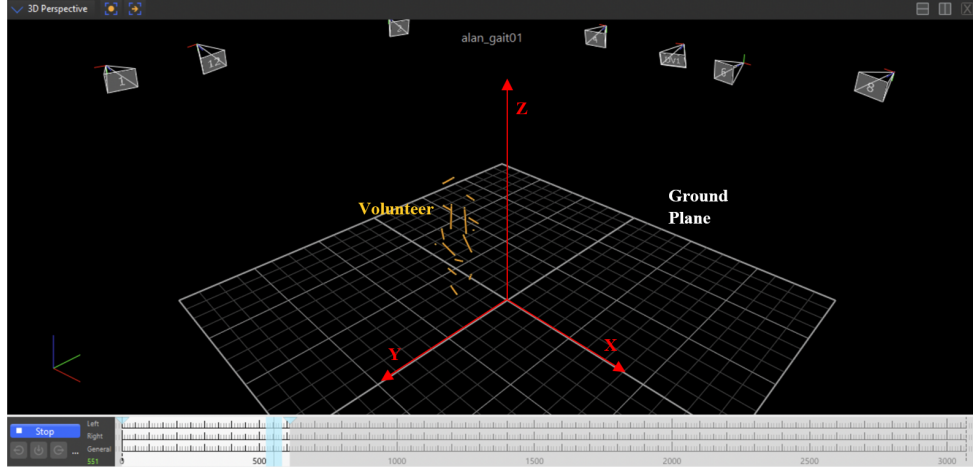


Figure 9 ViconNexus™ software GUI to visualise the PLW as it is being rendered

We called the `GetTrajectory` method on each of the 28 retro reflective nodes which were recorded in the motion capture lab. The method returned a $3 \times n$ array, where the three rows correlated to the x_i , y_i and z_i (Figure 9) coordinates respectively at each 10 millisecond time step (i). As our point light configuration contained 28 nodes (Section 2.1), we obtained 28 of these $3 \times n$ time-series, sampled at 100 Hz. We then labeled and saved each of the respective 28 arrays into their own separate .mat files. Doing so unlocked easy post processing of this raw data for our experiment.

3.3 PLW with Varying Viewpoint Angles

To visualise these nodes, we utilised an open source toolbox on MATLAB® named PsychToolBox. The features in this toolbox allow users to visualise captured visual stimuli for the purpose of testing in controlled environments. In our case, it allowed us to render 2D orthogonal representations. In addition, to allow for PLWs of different viewpoint angles, we needed to prepare the data by transforming it using the standard counter-clockwise rotation matrix (1, Appendix A.2).

$$\hat{x}_i' = \mathbf{M}_T \hat{x}_i \rightarrow \begin{bmatrix} x'_i \\ y'_i \\ z'_i \end{bmatrix} = \begin{bmatrix} \cos(\theta) & \sin(\theta) & 0 \\ -\sin(\theta) & \cos(\theta) & 0 \\ 0 & 0 & 1 \end{bmatrix} \begin{bmatrix} x_i \\ y_i \\ z_i \end{bmatrix} \quad (1)$$

Once the data had been manipulated into the desired form, PsychToolBox allowed us to render these coordinates onto the screen. It does so by translating the Cartesian coordinates we obtained from the MOCAP lab onto the pixel co-ordinates of our monitor. Computationally, it loops through each node's trajectory timeseries at the same frequency it was recorded (100Hz). By processing all 28 of these in parallel, we were then able to render the full PLW (Figure 10).

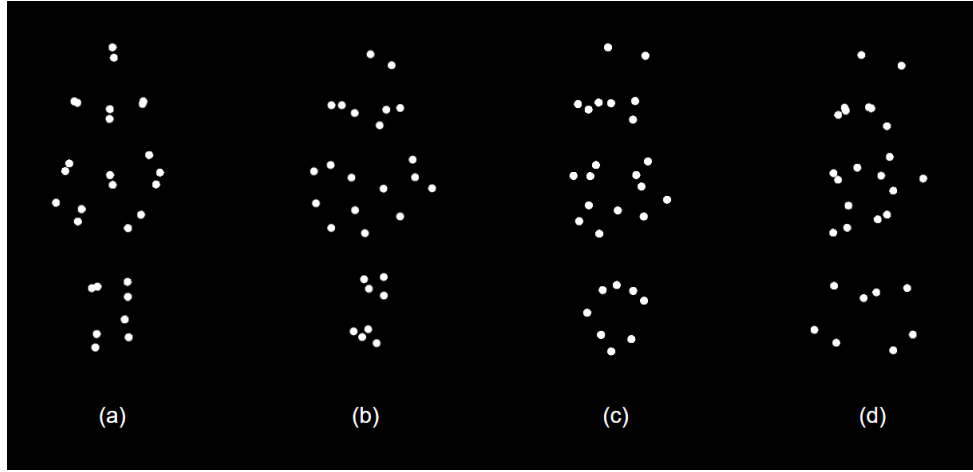


Figure 10 PLW with 28 visible nodes: (a) Angle = 0° , (b) Angle = 30° , (c) Angle = 60° , (d) Angle = 90°

3.4 PLW with Visual Degradation

We employed two visual degradation tactics to the four rendered PLWs shown above. The first was a function which could allow us to reduce the number of visible nodes for the rendered PLW (Figure 11). As this resolution is decreased, the coherence of the corresponding PLW is comprised.

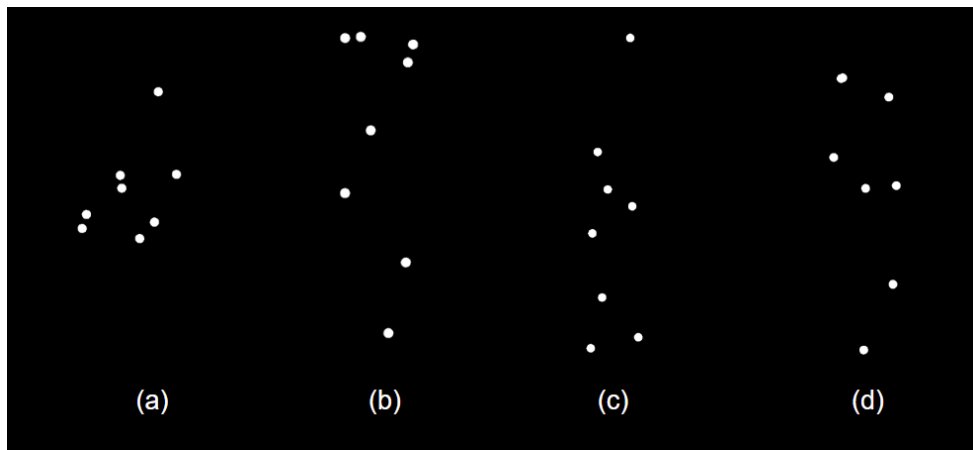


Figure 11 PLW with 8 visible nodes: (a) Angle = 0° , (b) Angle = 30° , (c) Angle = 60° , (d) Angle = 90°

Moreover, we implemented a node lifetime function. This feature assigned a random set of nodes every 200 milliseconds. In figure 11, all four PLWs are comprised of 8 nodes. However, note that the specific rendered nodes differ between stimuli. One can then imagine subsequent random sets of 8 new nodes being generated after this combination - at 50 millisecond intervals. The resulting animation of the PLW appears to "jitter", thereby adding to the visual degradation.

4. Experimental Methods

Once it was established that PLWs of various viewpoint angles and levels of degradation could be rendered, we moved onto the experimental design of our trials. We ensured our experiments could test for any possible differences in the performance of the PoBM with varying peripheral eccentricities. An experimental matrix was derived which became the framework of our trials. This framework was then used in a controlled testing environment to carry out the necessary experiments.

4.1 Experimental Matrix

For trialing purposes, we utilised a randomised matrix technique. This matrix would serve two main purposes. Firstly, for our experiment, it allowed us to select random configurations for subsequent PLWs. Secondly, we could store our data in an organised and systematic way. It was comprised of rows representing the number of dots (η_d), and columns representing the viewpoint angle (θ_v). To account for peripheral eccentricity (ϵ_d) in the testing structure, this was concatenated to the third dimension of the matrix (Figure 12). We used the following increments for these independent variables (Table 1):

Table 1 Independent Variables Table

Independent Variables	Increments
Viewpoint Angle, θ_v	0 30 60 90
Peripheral Eccentricity, ϵ_p	0 40
Number of Visible Dots, η_d	2 4 8 12 16 20 24

This matrix would represent a single block of trials, with its individual elements representing the trials it is comprised of. With this specific configuration, each whole block contained 56 individual trials (*rows* \times *columns* \times *layers*). Each of these trials comprised a unique combination of number of visible nodes, viewpoint angle and peripheral eccentricity (Figure 12). When conducting our experiment (Section 4.2), we could then populate each element of this 3D matrix with a "correct" boolean. This indicated whether the subject answered the specific combination correctly or incorrectly by assigning 1 or 0. We consider a trial complete when all 56 elements of this matrix have been assigned a value.

4.2 Experimental Design

In our experiment, we presented random elements of the 3D experimental matrix (Figure 12) consecutively. Each element rendered a PLW with a unique combination of viewpoint angle, number of visible nodes and peripheral eccentricity. Once presented by the stimuli, the observing subject is tasked with identifying the viewpoint angle of the PLW. This presented each trial as a four-alternative forced choice. Once all 56 trials were exhausted, a single block was completed. When performing our experiment, the subject completed four blocks in a row. As a result, each element of the final experimental matrix could have a maximum value of four.

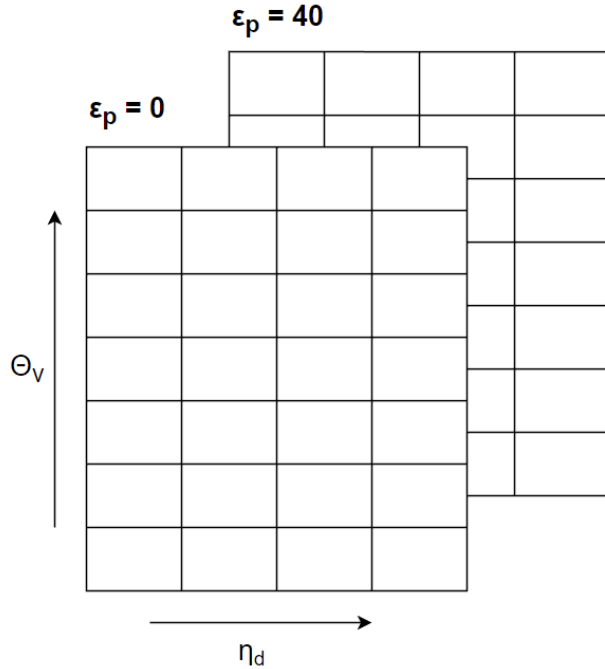


Figure 12 3D Experiment Matrix

4.2.1 Test Environment

To ensure the most fair and accurate results from our trial experiments, we set up the environment to be as controlled as possible. All trial experiments were done in the Brain Computer Interface (BCI) Lab and on the same test station. The BCI lab is equipped with strong acoustic and light insulation which allows it to be a consistently replicable testing environment. The subject was positioned with their head on a chin brace, which was located 50 cm away from a monitor (Figure 13a). This allowed for consistency in head location between all participating subjects.

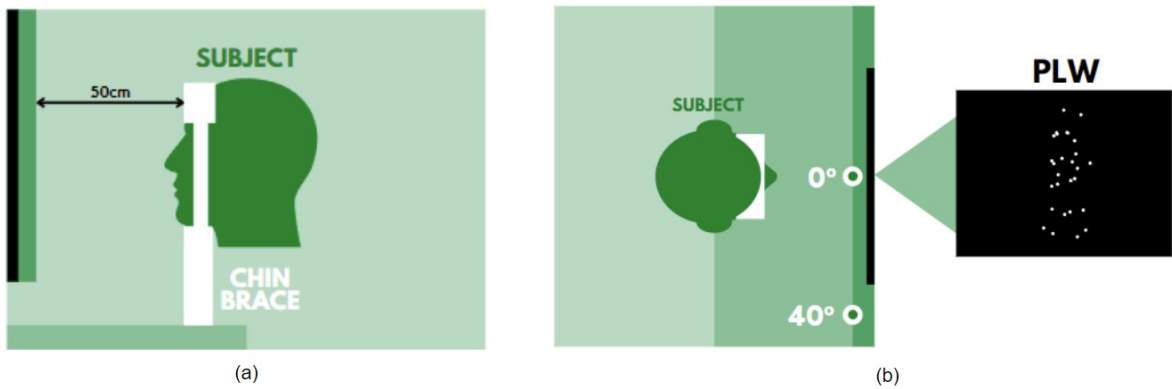


Figure 13 (a) Chin brace set up to control the movement of the subject's head, (b) Fixation spot at 0 and 40 degrees to indicate peripheral eccentricities

Positioned directly in front of the subject was a 27-inch monitor. Within the test environment there are two fixation spots [18]. One lies in the centre of the monitor and indicates a peripheral eccentricity of 0 degrees. The other lies 60 cm to the right of this, and indicates a peripheral eccentricity of 40 degrees (Figure 13b).

4.2.2 Test Procedure

Twelve participants volunteered for our trial experiments. All participants were members of the University of Auckland's Engineering department. These subjects were all acquainted with each other and worked in a close general vicinity over the course of the year.

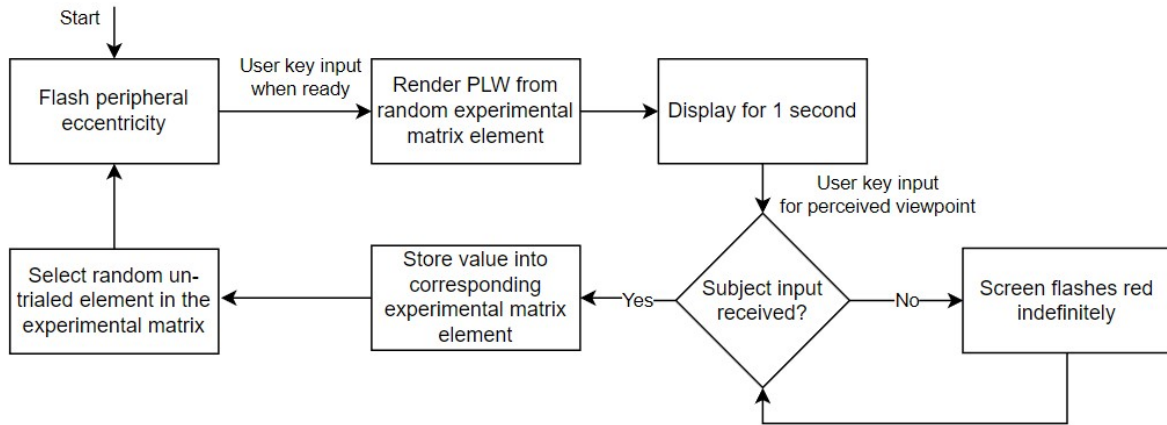


Figure 14 Flow diagram showing the designed test procedure. One full loop of this diagram indicates one completed trial in the overall block.

After the subjects were situated comfortably in the described test environment and a few test runs were given, we conducted the test procedure. The system we carried out was repeated for all test subjects in the same manner. First, the loop begins by displaying either 0° or 40° , to indicate the peripheral eccentricity angle which is being tested. The subject will then proceed to focus on the corresponding fixation point (Figure 13b). Once a user key input is received, a PLW will be generated with a random configuration of visible nodes and viewpoint angle as dictated by the experimental matrix.

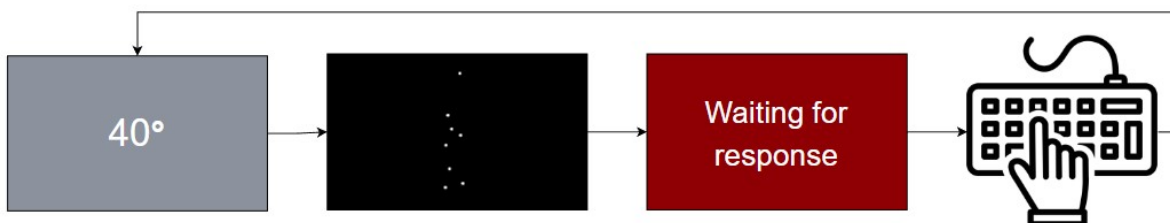


Figure 15 Visual diagram showing the progression of the trial loop.

The subject is then required to answer which viewpoint they perceived. If the subject does not do this within a 1 second time window, the screen will flash red indefinitely until the user input is received. This process repeats itself until all elements of the experimental matrix have been exhausted as discussed before.

5. Results and Discussion

Following the trial experiments, data analysis was done to quantify any effects changing peripheral eccentricity may have on the performance of the PoBM. Additionally, we analysed the relative performance differences between viewpoint angles. We fitted psychometric functions to relevant data and bootstrapped our samples to draw conclusions from our thresholds.

5.1 Foveal vs. Peripheral Vision

The results from all trial data suggests that peripheral eccentricity has a conclusive effect on the recognition accuracy of the PoBM. The overall performances at 0° and 40° eccentricity were found at each number of visible nodes (Figure 16). Success rate (ρ) was found by averaging the performance across all four viewpoint angles ($0^\circ, 30^\circ, 60^\circ, 90^\circ$) at each given number of nodes.

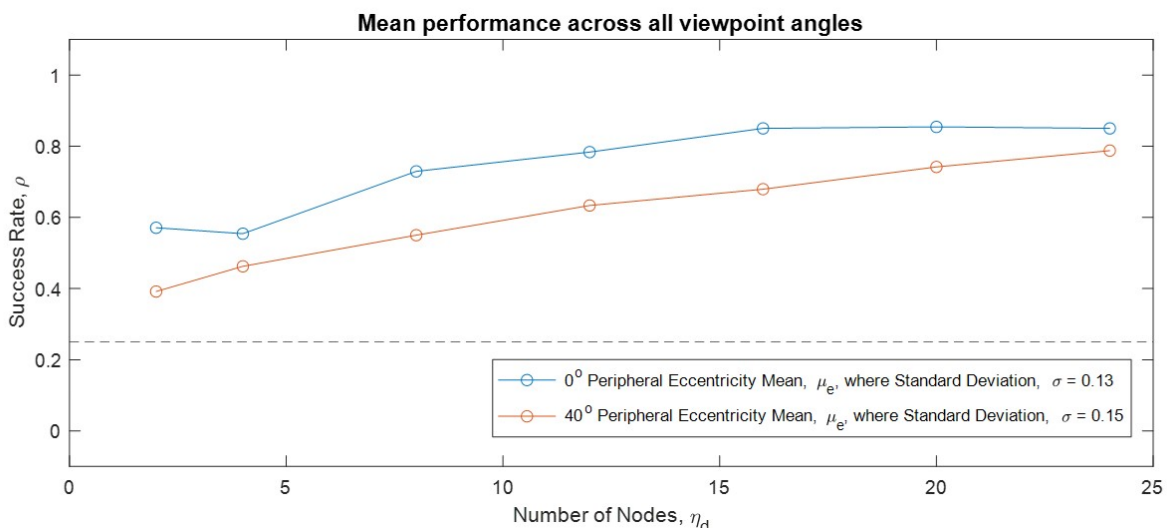


Figure 16 Mean success rate as a function of number of nodes

Qualitatively, it is clear that across all values of number of nodes, the success rate for 0° lies above 40° . This implies that on average, the success rate in the fovea will be higher with the same number of nodes. As expected, we see that the success rate clearly increases as the number of nodes representing the PLW increases.

5.1.1 Psychometric Functions

To quantify these differences in more meaningful ways, we plotted psychometric functions to the mean performance data of both peripheral eccentricity levels. The selected psychometric models were WCDFs [19] which are governed by the following equation:

$$P_{weibull} = \begin{cases} 0 & -\infty < x \leq \infty \\ 1 - e^{-x^\beta} & 0 < x < \infty, \beta > 0 \end{cases} \quad (2)$$

The least squares method [20] was then used to fit the function the data by ensuring that the sum of errors across the data points is minimised (Figure 17). We can see that these models asymptote to a value near perfect success rate (1.0). It can also be noted that the 0° curve reaches its asymptote much earlier.

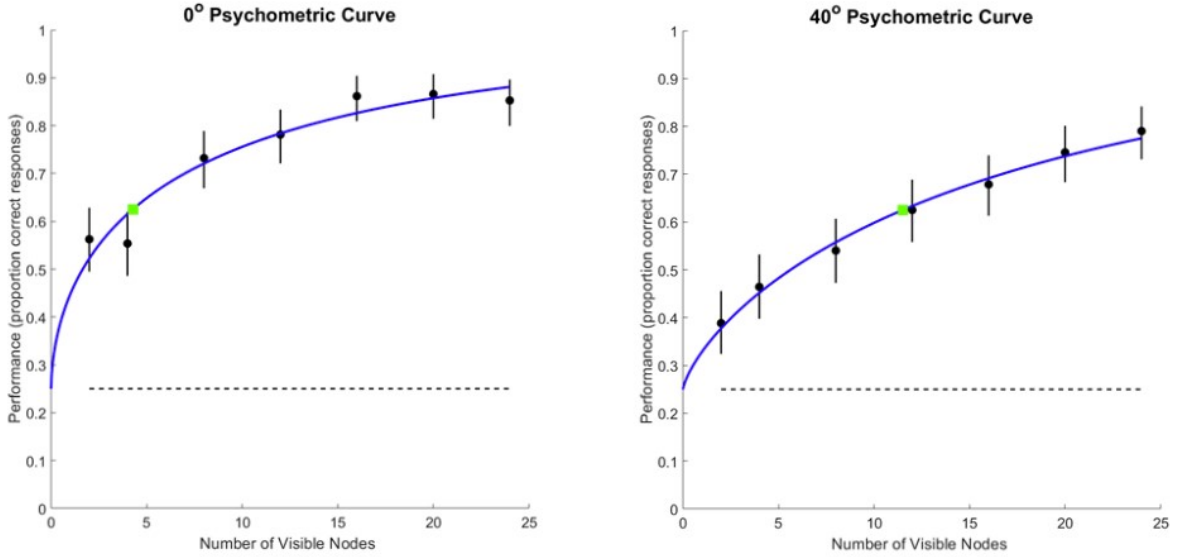


Figure 17 Fitted psychometric functions to the 0 and 40 degree eccentricity data. Indicated by green markers are the critical thresholds of each curve (4.276 and 11.508).

From these fitted psychometric functions we are able to obtain a value for the critical success rate. We define this as the point where the curves intersect a performance of 0.625, a value half-way between the guess rate (0.25) and perfect performance (1.0). This threshold represents the boundary for reliable PoBM as performance is significantly improved from the guess rate. At 0 degree eccentricity, this value is located at 4.28 nodes, while at 40 degree eccentricity, this value is 11.51 nodes. These two models provide insight into a potentially strong discrepancy between these two critical thresholds. This suggests that peripheral vision requires far more visual resolution for the same recognition accuracy of the PoBM.

5.1.2 Bootstrapping

In an effort to statistically prove this outcome, we bootstrapped our sample data 1000 times for both levels of peripheral eccentricity. Bootstrapping is a statistical procedure in which simulated samples are obtained by resampling an original dataset. In doing so, we were able to simulate 1000 different values for the critical success rate in our trial data.

The results of bootstrapping were plotted and further supported the conclusion that recognition accuracy is considerably better in the fovea compared to the periphery. As we can see, the bootstrapped data provided a Gaussian distribution in both sets of data. We obtained mean critical threshold values of 4.27 and 12.5 visible nodes for 0 and 40 degrees eccentricity respectively. These two groups have distributions which range from 2.4-6.1 and 9.1-14.3, which evidently do not overlap. Both these factors inform us of statistically significant differences between the recognition accuracy of PoBM between these two eccentricity levels.

This conclusion can be summarised by the following equation:

$$T_{C,0} < T_{C,40} \quad (3)$$

Where $T_{C,i}$ is the critical threshold in the i^{th} peripheral eccentricity.

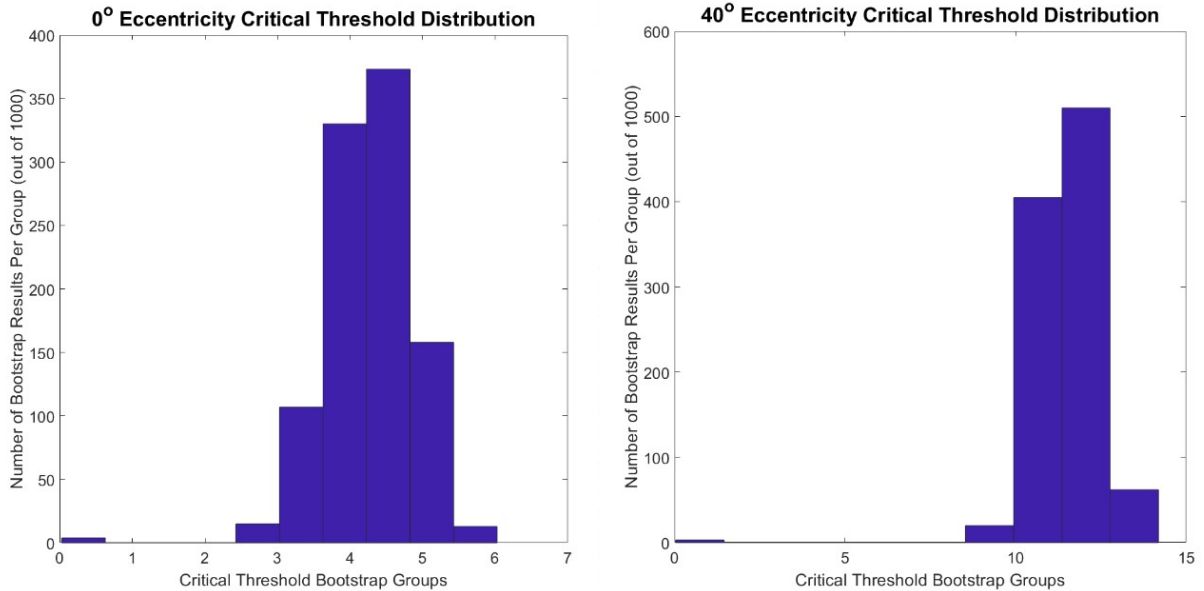


Figure 18 Histograms showing the Gaussian distribution of critical thresholds across 1000 rounds of bootstrapping. A 0 degree eccentricity has a mean value of 4.275 nodes and a 40 degree eccentricity has a mean value of 11.519 nodes.

5.2 Viewpoint Angle vs. Peripheral Eccentricity

We also investigated the specific interaction between individual viewpoint angles and peripheral eccentricity. Mainly, we noticed that peripheral vision may interact differently between frontal (0°) and profile (90°) viewpoints (Figure 19). As a result, we set out to quantify these results through statistical analysis using the same procedure as above.

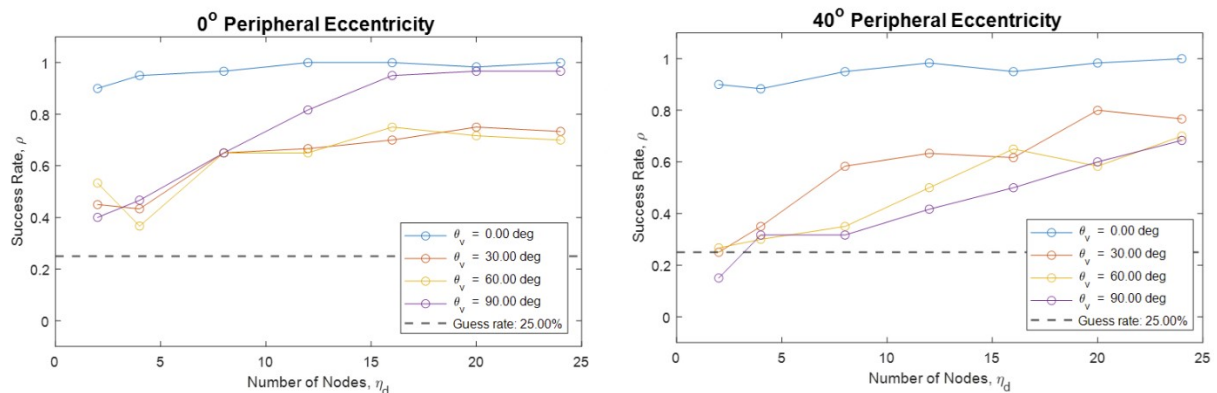


Figure 19 Raw data showing the success rate as a function of number of nodes for all four viewpoint angles

Qualitatively, we notice that frontal viewpoint performance remains highly accurate throughout the range of visible nodes. The recognition accuracy at this viewpoint angle also does not seem to vary with respect to peripheral eccentricity. In contrast, the data from profile viewpoint angles indicate a clear decrease in recognition accuracy between the fovea and periphery (Figure 19).

5.2.1 Psychometric Functions and Bootstrapping

We proceeded to fit the same WCDF functions (Figures B1, B2) to these individual viewpoint angles before bootstrapping to quantify any significant differences in the critical thresholds (Figures B3, B4). This was done for each combination of viewpoint angle and

peripheral eccentricity to test for any possible interactions, beyond what was immediately obvious upon observation. Each of the mean values for critical threshold was then found after bootstrapping (Table 2).

Table 2 Mean critical threshold values for each combination of viewpoint angle and peripheral eccentricity.

VIEWPOINT ANGLE (°)	PERIPHERAL	ECCENTRICITY (°)
	0	40
0	0.3118	0.1451
30	9.8595	12.9807
60	9.7043	14.4509
90	6.8052	16.9332

The first noticeable feature is a very low critical threshold (0.3118 and 0.1451 respectively) for frontal viewpoints at both eccentricity levels. Our fitted models seem to predict that observers require less than a single visible node to know when biological motion is approaching them. This can be explained from an evolutionary lens - humans may have developed a heightened sense of awareness as a predator/prey moved directly towards them. Those who reacted to this type of biological motion survived, while those who did not fell prey. In the case of our experiment, the 2D orthogonal representation means that there is almost no displacement of the arms from left to right. This may be a key indicator for higher sensitivity [4]. This result could also indicate slight flaws in the experimental method. It can be hypothesised that trialing subjects defaulted to answering a viewpoint angle of 0° when they were unsure.

Secondly, we found that the critical threshold for side-profile viewpoints (30° and 60°) are comparable. These values are slightly closer in the fovea than in the periphery, but the difference is small. We conclude that this may be due to confusion between the two viewpoint angles. Among many subjects, a common piece of feedback was that these side-profile angles were especially difficult to discern from each other.

Finally, the statistical analysis shows that profile viewpoints are markedly more recognisable in the fovea. The mean for the critical threshold in the fovea was 6.805 compared to 16.933 in the periphery. In addition, there was no overlap between either range of bootstrapped mean values. Here we hypothesise that the reduction in acuity in the periphery is highly detrimental to PoBM discernment. It can be noted that the mean value for the critical threshold in the periphery is much closer to those of the side-profile angles. This perhaps suggests that in the periphery, subject's become confused and mix up all three of these viewpoint angles.

These two conclusions can be summarised by the following equations:

$$T_{C(frontal),fovea} \approx T_{C(frontal),periphery} \ll T_{C(others)} \quad (4)$$

$$T_{C(profile),fovea} \ll T_{C(profile),periphery} \quad (5)$$

For future studies we recommend that the subject's specific viewpoint angle input is recorded, such that false positives can be recorded. Using a confusion matrix, typically analysis can be done by calculating values like specificity, sensitivity and accuracy. Further analysis can be done by calculating parameters like the Matthews Correlation Coefficient (MCC) to better understand potential flaws [21]. Before this is done, the discussed results should be taken with a degree of caution.

6. Conclusion

In this project, we set out to quantify any interactions between the performance of the PoBM and changing peripheral eccentricities. Following our trial experiments, we conducted data analysis to draw conclusions for our proposed hypothesis. We found that there was significant reduction in recognition accuracy for subjects in the periphery. After 1000 rounds of bootstrapping, we found that the mean critical threshold in the periphery was 11.519 nodes. Given the mean critical threshold in the fovea was 4.275, there is over a 7 node difference between the two values. There are 28 nodes for the full configuration, thus this difference accounts for a quarter of the nodes on our PLW. This is a significant proportion of the resolution, meaning our experiments provide a confident conclusion to our hypothesis.

These results translate to real life scenarios observed in various situations. From intuition and our personal experiences, acuity in the peripheral vision clearly diminishes. In sport, we often focus our gaze upon targets to make use of the higher levels of acuity in our foveal vision [22]. In reading and writing, we always use the foveal part of our visual field. Studies have shown that the performance for both these activities are qualitatively inferior in the periphery [23]. Our project has provided near equivalent insight for the paradigm of biological motion.

Furthermore, we noticed some interesting features by analysing the recognition accuracy of different viewpoint angles individually. We found that the results for a viewpoint angle of 0 degrees at both levels of peripheral eccentricity suggest extremely high sensitivity. Additionally, we found that recognition accuracy for a viewpoint angle of 90 degrees greatly improved in the foveal. As discussed previously, it should be reiterated that until these results are presented in confusion matrices, they should be taken with caution.

7. Future Works

The work done in this project provides a baseline which can be built upon in several different directions. The research done here has taken on a scientific focus. This was deemed necessary due to the limited literature surrounding our scope. Future works may progress this further - or it may pivot to a project more focused on practical engineering applications.

Some suggestions for potential future works are:

- Present 4x4 confusion matrices for the trial data which inputs specific viewpoint angle responses. One side of the matrix represents the displayed viewpoint angles and the other side represents the responded viewpoint angles.
- Using these specific responses we analyse how exactly responses are being answered incorrectly. For example, qualitatively, we can inspect with greater clarity whether subject's were defaulting to a viewpoint angle of 0 degrees when they did not know. Quantitatively, we can then calculate parameters such as MCC to quantify these features.
- At present, viewpoint angle is being altered in the azimuth direction. The transformation matrix (1) allows for variation in elevation. To gain a full perspective on how viewpoint angle and peripheral eccentricity effect the PoBM, it would be worth

testing all dimensions in the spherical co-ordinate system. This research could unlock a wider scope of practical engineering applications [24].

- Create a machine learning model for the PoBM [25, 26] which can be used predict viewpoint angles as we had our trial subjects do. The project can then proceed to compare the differences in recognition accuracy between the trained model's PoBM and human PoBM.
- Apply engineering applications to the PoBM. In more recent times, literature in the PoBM has extended into fields like health and safety, sport, military, etc. [27–30]. These studies have worked to optimise visual markers for biological motion to ensure that critical subjects are as visible as possible. Students may choose to explore similar fields, or one that has not been done before.

References

- [1] G. Johansson, “Visual perception of biological motion and a model for its analysis,” *Perception & psychophysics*, vol. 14, no. 2, pp. 201–211, 1973.
- [2] S. V. Stevenage, M. S. Nixon, and K. Vince, “Visual analysis of gait as a cue to identity,” *Applied Cognitive Psychology: The Official Journal of the Society for Applied Research in Memory and Cognition*, vol. 13, no. 6, pp. 513–526, 1999.
- [3] N. F. Troje and C. Westhoff, “The inversion effect in biological motion perception: Evidence for a âlife detectorâ?” *Current biology*, vol. 16, no. 8, pp. 821–824, 2006.
- [4] S. M. Thurman and E. D. Grossman, “Temporal âbubblesâ reveal key features for point-light biological motion perception,” *Journal of Vision*, vol. 8, no. 3, pp. 28–28, 2008.
- [5] C. D. Barclay, J. E. Cutting, and L. T. Kozlowski, “Temporal and spatial factors in gait perception that influence gender recognition,” *Perception & psychophysics*, vol. 23, no. 2, pp. 145–152, 1978.
- [6] G. Mather and L. Murdoch, “Gender discrimination in biological motion displays based on dynamic cues,” *Proceedings of the Royal Society of London. Series B: Biological Sciences*, vol. 258, no. 1353, pp. 273–279, 1994.
- [7] N. F. Troje, “Decomposing biological motion: A framework for analysis and synthesis of human gait patterns,” *Journal of vision*, vol. 2, no. 5, pp. 2–2, 2002.
- [8] L. T. Kozlowski and J. E. Cutting, “Recognizing the sex of a walker from a dynamic point-light display,” *Perception & psychophysics*, vol. 21, no. 6, pp. 575–580, 1977.
- [9] Y. Ma, H. M. Paterson, and F. E. Pollick, “A motion capture library for the study of identity, gender, and emotion perception from biological motion,” *Behavior research methods*, vol. 38, no. 1, pp. 134–141, 2006.
- [10] N. F. Troje, “The little difference: Fourier based synthesis of gender-specific biological motion,” *Dynamic perception*, pp. 115–120, 2002.
- [11] N. F. Troje, C. Westhoff, and M. Lavrov, “Person identification from biological motion: Effects of structural and kinematic cues,” *Perception & Psychophysics*, vol. 67, no. 4, pp. 667–675, 2005.
- [12] A. Freire, T. L. Lewis, D. Maurer, and R. Blake, “The development of sensitivity to biological motion in noise,” *Perception*, vol. 35, no. 5, pp. 647–657, 2006.
- [13] G. Mather and S. West, “Recognition of animal locomotion from dynamic point-light displays,” *Perception*, vol. 22, no. 7, pp. 759–766, 1993.
- [14] R. Rosenholtz, “Capabilities and limitations of peripheral vision,” *Annual review of vision science*, vol. 2, pp. 437–457, 2016.
- [15] H. Strasburger, I. Rentschler, and M. Jüttner, “Peripheral vision and pattern recognition: A review,” *Journal of vision*, vol. 11, no. 5, pp. 13–13, 2011.
- [16] C. A. Curcio, K. R. Sloan, R. E. Kalina, and A. E. Hendrickson, “Human photoreceptor topography,” *Journal of comparative neurology*, vol. 292, no. 4, pp. 497–523, 1990.

- [17] G. Osterberg, “Topography of the layer of the rods and cones in the human retina,” *Acta ophthalmol*, vol. 13, no. 6, pp. 1–102, 1935.
- [18] H. Ikeda, R. Blake, and K. Watanabe, “Eccentric perception of biological motion is unscalably poor,” *Vision research*, vol. 45, no. 15, pp. 1935–1943, 2005.
- [19] K. Zchaluk and D. H. Foster, “Model-free estimation of the psychometric function,” *Attention, Perception, & Psychophysics*, vol. 71, no. 6, pp. 1414–1425, 2009.
- [20] K. Levenberg, “A method for the solution of certain non-linear problems in least squares,” *Quarterly of applied mathematics*, vol. 2, no. 2, pp. 164–168, 1944.
- [21] D. Chicco, N. Tötsch, and G. Jurman, “The matthews correlation coefficient (mcc) is more reliable than balanced accuracy, bookmaker informedness, and markedness in two-class confusion matrix evaluation,” *BioData mining*, vol. 14, no. 1, pp. 1–22, 2021.
- [22] C. Vater, R. Kredel, and E.-J. Hossner, “Examining the functionality of peripheral vision: From fundamental understandings to applied sport science,” *Current Issues in Sport Science*, vol. 2, no. 010, 2017.
- [23] K. Latham and D. Whitaker, “A comparison of word recognition and reading performance in foveal and peripheral vision,” *Vision Research*, vol. 36, no. 17, pp. 2665–2674, 1996.
- [24] J. Martinez, R. Hossain, J. Romero, and J. J. Little, “A simple yet effective baseline for 3d human pose estimation,” in *Proceedings of the IEEE International Conference on Computer Vision (ICCV)*, Oct 2017.
- [25] M. Sadeghi, F. Schrodt, S. Otte, and M. V. Butz, “Gestalt perception of biological motion: A generative artificial neural network model,” in *2021 IEEE International Conference on Development and Learning (ICDL)*. IEEE, 2021, pp. 1–7.
- [26] M. H. Mozaffari and W.-S. Lee, “Semantic segmentation with peripheral vision,” in *International Symposium on Visual Computing*. Springer, 2020, pp. 421–429.
- [27] J. M. Wood, R. A. Tyrrell, R. Marszalek, P. Lacherez, A. Chaparro, and T. W. Britt, “Using biological motion to enhance the conspicuity of roadway workers,” *Accident Analysis & Prevention*, vol. 43, no. 3, pp. 1036–1041, 2011.
- [28] K. Steel, E. Ellem, and D. Baxter, “The application of biological motion research: biometrics, sport, and the military,” *Psychonomic bulletin & review*, vol. 22, no. 1, pp. 78–87, 2015.
- [29] J. M. Wood, R. Marszalek, P. Lacherez, and R. A. Tyrrell, “Configuring retroreflective markings to enhance the night-time conspicuity of road workers,” *Accident Analysis & Prevention*, vol. 70, pp. 209–214, 2014.
- [30] J. M. Wood, R. Marszalek, P. Lacherez, R. A. Tyrrell, and A. Chaparro, “Perceptions of visibility and conspicuity of biomotion clothing configurations for road workers at road work sites,” in *Transportation Research Board 89th Annual Meeting*, 2010.

Appendix A The First Appendix

A.1 MATLAB Data Processing

weibull_psych_fit.m

```
1 function crit = psych_fit_weibull(DATA)
2 % DATA = subject success input (1 = success, 0 = fail)
3
4 % Visual degradation
5 NOISE = [2 4 8 12 16 20 24];
6 NOISE_ = linspace(0,max(NOISE),1000);
7
8 % Inline functions
9 fnBound = @(bhat) 1/(eps+double((bhat(1) > 0) & (bhat(2) > 0)));
10 fnPsychometric = @(lam,k,x) 0.25 + 0.75*(1 - exp(-power(max(0,x)/lam
11 ,k)));
11 fnCost = @(bhat) sum(power(fnPsychometric(bhat(1),bhat(2),NOISE) -
12 mean(DATA,1),2)) * fnBound(bhat);
13
14 % Find lowest cost function
15 best_fval = 1/eps;
16 for iistart = 1:1000
17     BHATO = [3 1];
18     if (iistart > 1)
19         BHATO = [2+4*rand() 3*rand()];
20     end
21     [bhat,fval] = fminsearch(fnCost, BHATO);
22     if (fval < best_fval)
23         best_fval = fval;
24         best_bhat = bhat;
25     end
26 end
27
28 % Fit psychometric curve
29 PM_ = fnPsychometric(bhat(1),bhat(2),NOISE_);
30
31 % Determine threshold, that is, where the fitted function = 0.625
32 crit = NOISE_(min(find(PM_ > 0.625)));
33
```

bootstrap_conf_int.m

```
1 % Load data
2 load("total_fourty.mat")
3 load("total_zero.mat")
4
5 % Define vars
6 BOOT = 1000;
7 DATA = totalZeroArray;
8
9 % Bootstrap and store crit
10 for dat = 1:2
11     for NBOOT = 1:BOOT
12         for deg = 1:size(DATA,2)
13             data = DATA(:, deg);
14             ix = ceil(length(data)) * rand(length(data),1);
```

```

15         data_{dat}(:, deg) = data(ix); % resample _with_ replacement
16     end
17     crit(NBOOT, dat) = psych_fit_weibull(data_{dat});
18 end
19 DATA = totalFourtyArray;
20 end
21
22 % Plot data
23 close all;
24 figure; hist(crit(:,1)); axis square
25 title("0^o Eccentricity Critical Threshold Distribution", FontSize=24)
26 ylabel(sprintf("Number of Bootstrap Results Per Group (out of %.0f)",
    BOOT))
27 xlabel("Critical Threshold Bootstrap Groups")
28 figure; hist(crit(:,2)); axis square
29 title("40^o Eccentricity Critical Threshold Distribution", FontSize=24)
30 ylabel(sprintf("Number of Bootstrap Results Per Group (out of %.0f)",
    BOOT))
31 xlabel("Critical Threshold Bootstrap Groups")

```

A.2 Data Collection and Stimuli Construction

biowalker_trials.m

```

1 %% PSYCH SETUP
2 % Clear the workspace and the screensca
3
4 sca;
5 close all;
6 clearvars;
7
8 % Here we call some default settings for setting up Psychtoolbox
9 PsychDefaultSetup(2);
10
11 % Set window to opacity for debugging
12 PsychDebugWindowConfiguration(0, 1);
13
14 % Get the screen numbers
15 screens = Screen('Screens');
16 screenNumber = max(screens);
17
18 % Open an on screen window
19 [window, windowRect] = PsychImaging('OpenWindow', screenNumber, [200 200
    200]);
20
21 % Get the size of the on screen window
22 [screenXpixels, screenYpixels] = Screen('WindowSize', window);
23
24 % Query the frame duration
25 ifi = Screen('GetFlipInterval', window);
26
27 %% TRIAL MATRIX SETUP
28 num_trials = 4;
29 theta_v = [90, 120, 150, 180];
30 degradation = [2,4,8,12,16,20,24];
31 eccentricity = [0, 40];
32
33 trial_rand = {};
34

```

```

35 for i = 1:num_trials
36     trial_rand = [trial_rand, randomiseTrials(theta_v, degradation,
37         eccentricity)];
38 end
39 %% DOT SETUP2
40 % Colour intensity
41 colourLevel = 1;
42
43 % We can define a center for the dot coordinates to be relative to.
44 % Here
45 % we set the centre to be the centre of the screen
46 trueDotCenter = [(screenXpixels / 2) (screenYpixels / 2)];
47 dotCenter = [(screenXpixels / 2 - 140) (screenYpixels / 2 + 500)];
48 dotYpos = 0;
49 dotXpos = 0;
50 dotSizes = 10;
51
52 white = WhiteIndex(screenNumber);
53 dotColours = white*colourLevel;
54
55 % Sync us and get a time stamp
56 Screen('Flip', window);
57 waitframes = 1;
58
59 % Maximum priority level
60 topPriorityLevel = MaxPriority(window);
61 Priority(topPriorityLevel);
62
63 % Draw White Dot on screen
64 Screen('DrawDots', window, [dotXpos; dotYpos], dotSizes, dotColours,
65     trueDotCenter, 2);
66 Screen('Flip', window);
67
68 time = 0;
69 data_count = 1;
70 life_count = 0;
71
72 len = 1000;
73 scale = 2;
74
75 inputKey = cell(1, size(theta_v, 2)*size(degradation, 2));
76
77 for trial = 1:size(trial_rand, 2)
78     % Flash grey
79     Screen('TextFont', window, 'Arial Unicode MS');
80     Screen('TextSize', window, 125);
81     DrawFormattedText(window, num2str(trial_rand{trial}.eccentricity), '
82         Center', 'Center', [0, 0, 0]);
83     Screen('Flip', window);
84
85     KbStrokeWait;
86
87     % Reset black
88     Screen('FillRect', window, [0, 0, 0]);
89
90     Screen('Flip', window);
91
92     trajData = getTrajData(trial_rand{trial}.degradation, trial_rand{

```

```

        trial}.theta_v, 'TrajectoryData/*.mat', scale);
91    while (~validKey(trial_rand{trial}.inputKey))
92        [~, ~, keyCode, ~] = KbCheck;
93        trial_rand{trial}.inputKey = KbName(keyCode);
94
95        if (mod(life_count, len/50) == 0)
96            trajData = getTrajData(trial_rand{trial}.degradation,
97                trial_rand{trial}.theta_v, 'TrajectoryData/*.mat', scale)
98                ;
99
100       end
101
102       % Extract dotXpos and dotYpos and apply to dot on screen
103       if time <= 1
104           for i = 1:length(trajData)
105               dotXpos = trajData{2, i}.array(1, data_count)/scale;
106               dotYpos = -trajData{2, i}.array(3, data_count)/scale;
107               Screen('DrawDots', window, [dotXpos; dotYpos], dotSizes,
108                   white, dotCenter, 2);
109           end
110       else
111           Screen('FillRect', window, [0.5, 0, 0]);
112       end
113
114       % Flip to the screen
115       Screen('Flip', window);
116
117       % Increment the time
118       time = time + ifi;
119
120       data_count = incrementValues(data_count, time) + 1;
121       life_count = incrementValues(life_count, time);
122
123       data_count = 1;
124       pause(0.5);
125
126       trial_rand = populateCorrect(trial_rand, trial, trial_rand{trial}.
127           inputKey);
128       time = 0;
129   end
130
131   % Clear screen
132   sca;
133
134   matrix = dataParser(trial_rand, theta_v, degradation, eccentricity);
135
136   % Keep useful vars
137   clearvars -except matrix num_trials;
138
139   name = input("Trial Subject Name: ", "s");
140   cd TrialData/Store/
141   save(sprintf("%s-%s.mat", date, name))
142   cd ../..

```

rotate_axis.m

```
1 function traj3Drot = rotateAxis(traj3D, theta, vp)
2     if (vp == "overhead")
3         % Rotation Matrix for overhead rotation
4         A = [1 0 0; 0 cosd(theta) -sind(theta); 0 sind(theta) cosd(theta)
5             ];
6         traj3Drot = A*traj3D;
7     elseif (vp == "profile")
8         % Rotation Matrix for profile rotation
9         A = [cosd(theta) sind(theta) 0; -sind(theta) cosd(theta) 0; 0 0
10            ];
11         traj3Drot = A*traj3D;
12     end
13 end
```

Appendix B Second Appendix

B.1 Viewpoint Graphs

B.1.1 Viewpoint Psychometric Functions

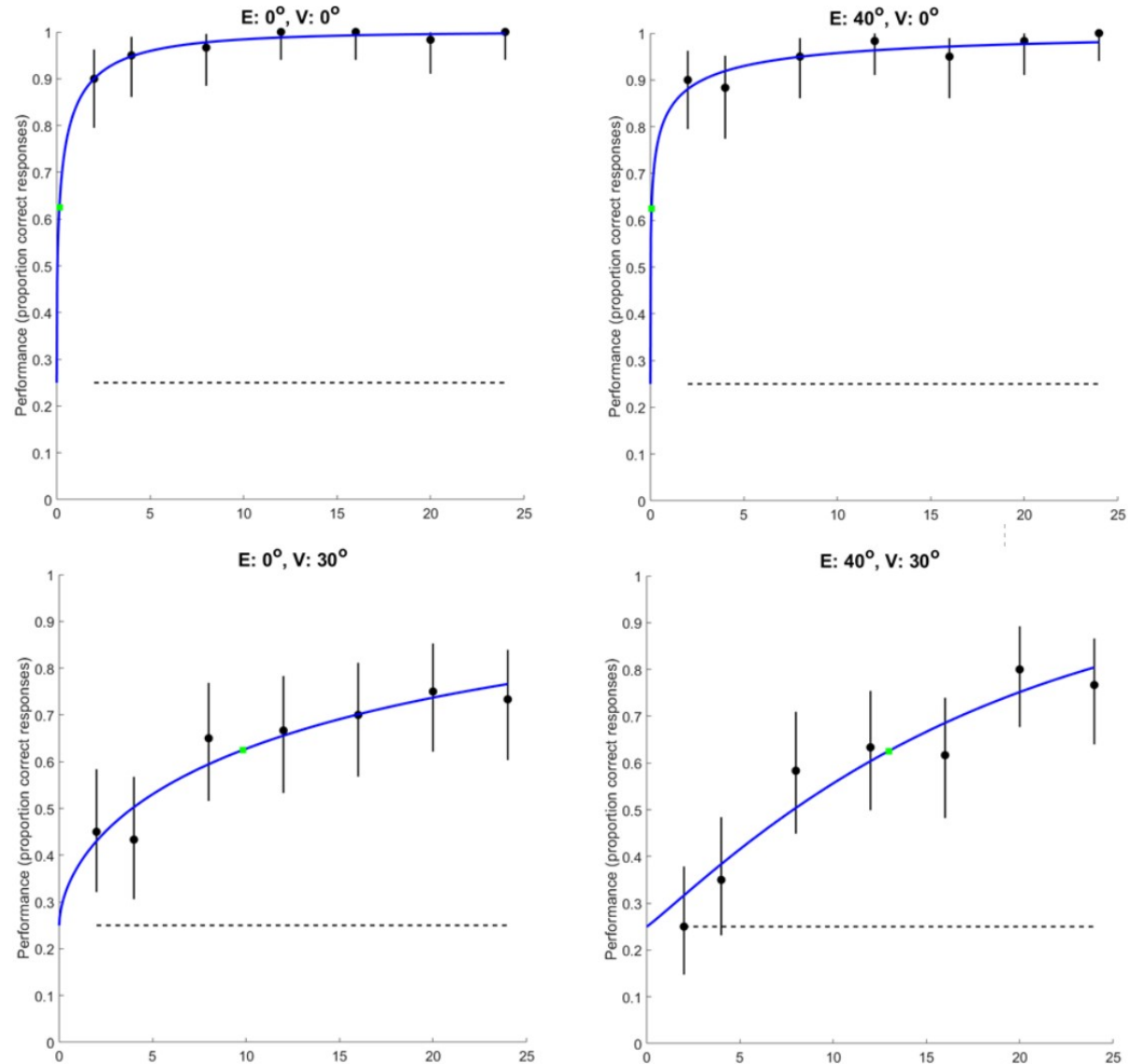


Figure B1 Psychometric functions between viewpoint angles of 0 and 30 degrees

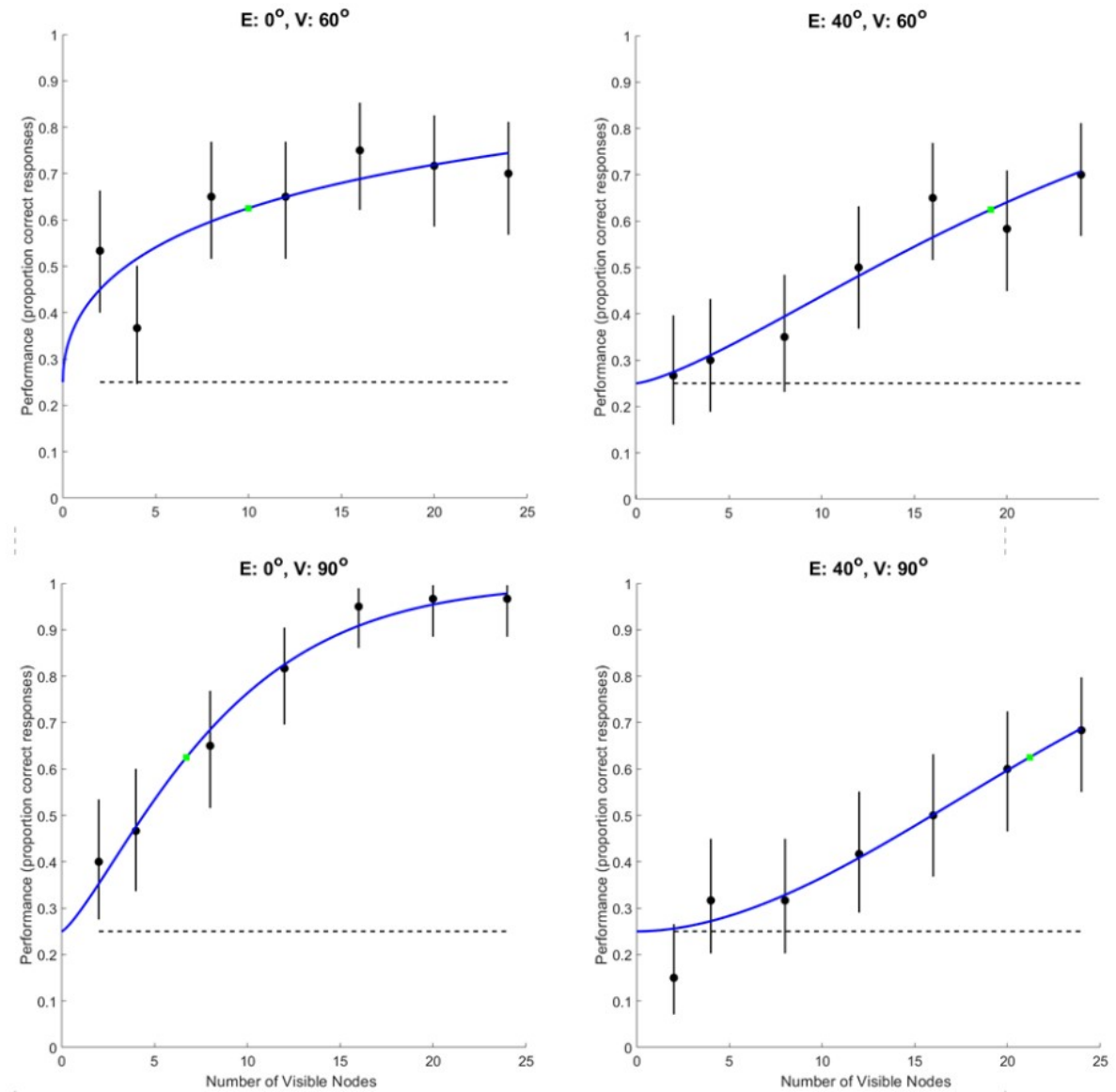


Figure B2 Psychometric functions between viewpoint angles of 60 and 90 degrees

B.1.2 Viewpoint Bootstrapped Histograms

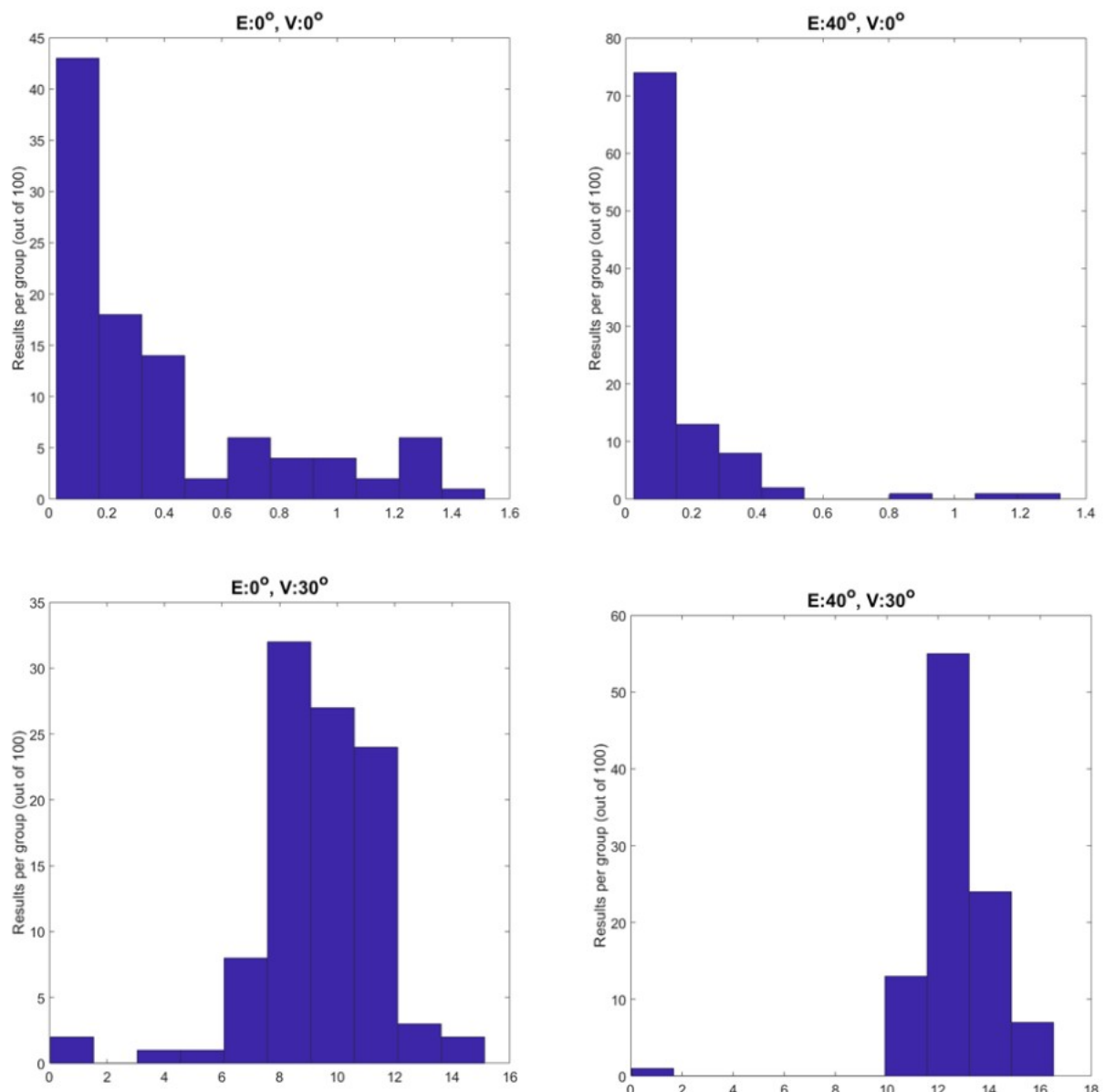


Figure B3 Bootstrapped histograms between viewpoint angles of 0 and 30 degrees

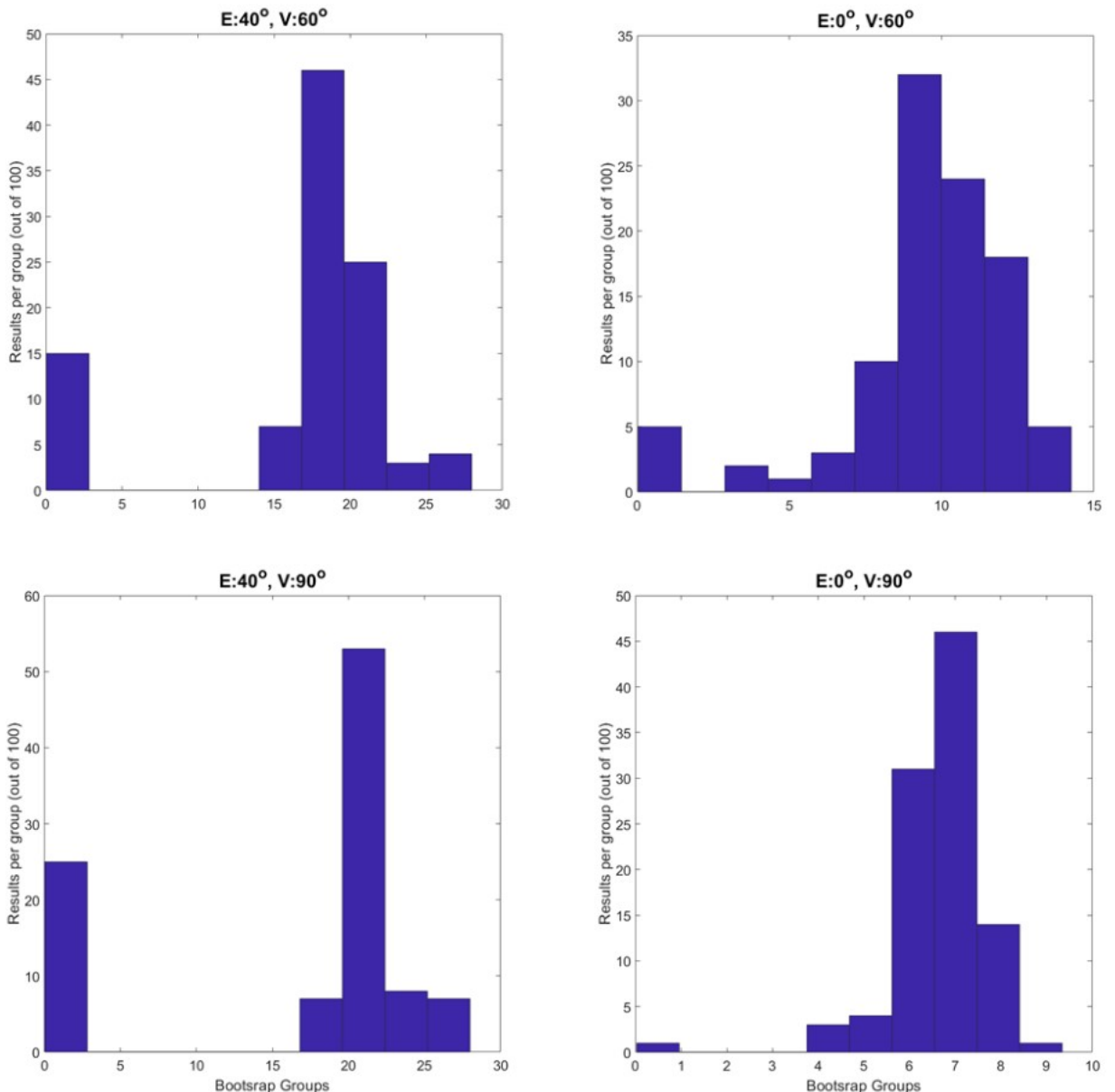


Figure B4 Bootstrapped histograms between viewpoint angles of 60 and 90 degrees

Appendix C MOCAP Lab

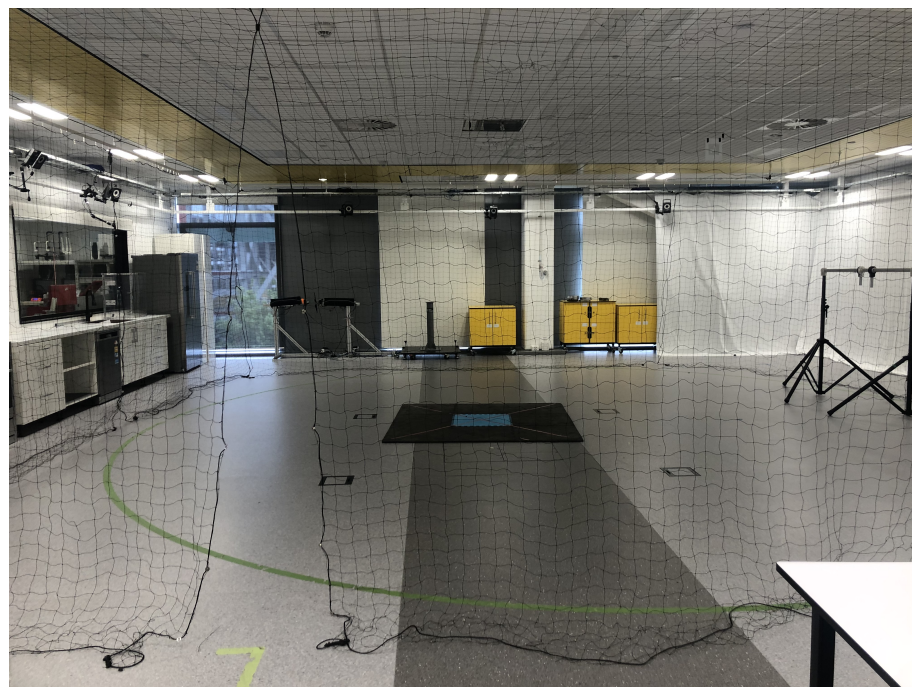


Figure C5 Motion capture lab at the University of Auckland

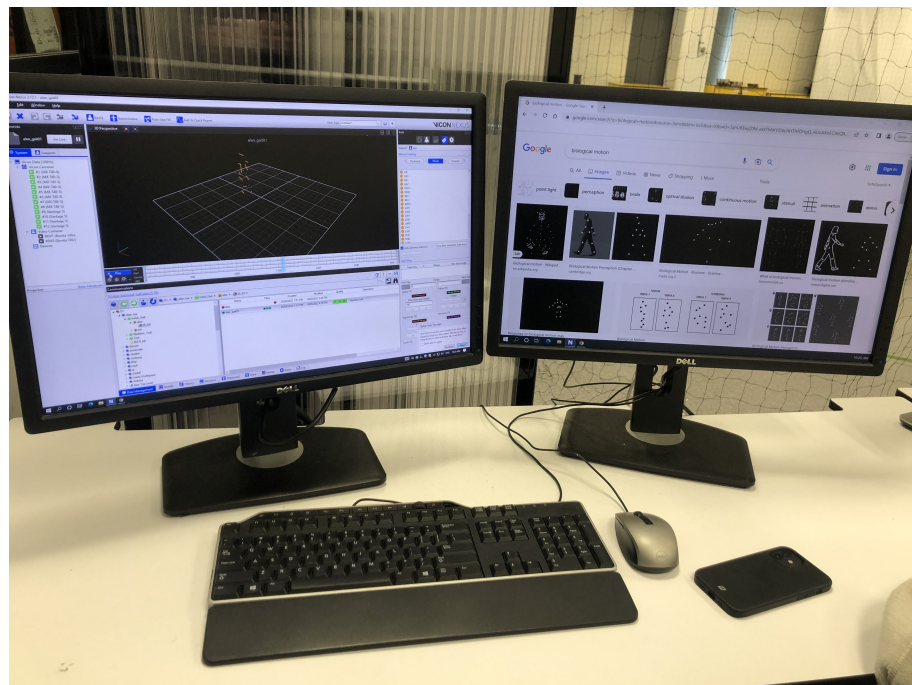


Figure C6 Vicon Nexus station which interfaces with the system which connects all the cameras within the lab

Appendix D Test Environment



Figure D7 BCI Lab station where all trial experiments are done (note: lights switched off under normal test conditions)